Available online at www.sciencedirect.com

ScienceDirect

Geochimica et Cosmochimica Acta 122 (2013) 209–225

Geochimica et Cosmochimica Acta

www.elsevier.com/locate/gca

Ca, Sr, O and D isotope approach to defining the chemical evolution of hydrothermal fluids: Example from Long Valley, CA, USA

Shaun T. Brown [a,b,*], B. Mack Kennedy [a], Donald J. DePaolo [a,b], Shaul Hurwitz [c], William C. Evans [c]

[a] *Earth Sciences Division, Lawrence Berkeley National Laboratory, Berkeley, CA 94720, United States*
[b] *Earth and Planetary Science, University of California, Berkeley, Berkeley, CA 94720, United States*
[c] *U.S. Geological Survey, Menlo Park, CA 94025, United States*

Received 31 December 2012; accepted in revised form 15 August 2013; Available online 4 September 2013

Abstract

We present chemical and isotopic data for fluids, minerals and rocks from the Long Valley meteoric-hydrothermal system. The samples encompass the presumed hydrothermal upwelling zone in the west moat of the caldera, the Casa Diablo geothermal field, and a series of wells defining a nearly linear, ~16 km long, west-to-east trend along the likely fluid flow path. Fluid samples were analyzed for the isotopes of water, Sr, and Ca, the concentrations of major cations and anions, alkalinity, and total CO_2. Water isotope data conform to trends documented in earlier studies, interpreted as indicating a single hydrothermal fluid mixing with local groundwater. Sr isotopes show subtle changes along the flow path, which requires rapid fluid flow and minimal reaction between the channelized fluids and the wallrocks. Sr and O isotopes are used to calculate fracture spacing using a dual porosity model. Calculated fracture spacing and temperature data for hydrothermal fluids indicate the system is (approximately) at steady-state. Correlated variations among total CO_2, and the concentration and isotopic composition of Ca suggest progressive fluid degassing (loss of CO_2), which drives calcite precipitation as the fluid flows west-to-east and cools. The shifts in Ca isotopes require that calcite precipitated at temperatures of 150–180 °C is fractionated by ca. −0.3‰ to −0.5‰ relative to aqueous species. Our data are the first evidence that Ca isotopes undergo kinetic fractionation at high temperatures (>100 °C) and can be used to trace calcite precipitation along hydrothermal fluid flow paths.
Published by Elsevier Ltd.

1. INTRODUCTION

The chemical composition of a hydrothermal fluid records the net product of mineral dissolution, precipitation, ion exchange, sorption, fluid mixing and vapor loss, but does not fully constrain the relative importance of each process along the fluid flow path. Chemical reactive transport models can provide a quantitative treatment of fluid flow that incorporates both hydrology and chemistry, but they are limited in their ability to adequately constrain appropriate chemical reaction paths and rates in natural systems often due to complex mineral assemblages and poorly constrained reactive surface area. For example, the well-known discrepancy between the geophysical and various geochemical estimates of hydrothermal fluid flux at ocean ridges largely arises due to limited knowledge of off-axis hydrothermal reactions and fluid pathways (e.g., Alt, 1995; Elderfield and Schultz, 1996; Coumou et al., 2008). New and improved geochemical techniques that can better probe the chemical and physical processes in fluid-rock reservoirs could improve models of hydrothermal systems, leading to more accurate reactive transport models.

* Corresponding author.
E-mail address: stbrown@lbl.gov (S.T. Brown).

0016-7037/$ - see front matter Published by Elsevier Ltd.
http://dx.doi.org/10.1016/j.gca.2013.08.011

The stable isotopes of water ($^{18}O/^{16}O$ and D/H) and sulfur have been used extensively to study hydrothermal systems, fossil hydrothermal systems, and ore deposits (e.g., Ohmoto, 1972; Magaritz and Taylor, 1976; Taylor and Forester, 1979). Isotope ratios of solute species such as Sr, Nd, Pb, Ca, Cl, C, and U, also offer promising yet still under-utilized tools for elucidating important chemical and physical reactions in hydrothermal systems (e.g., Doe and Zartman, 1979; Kaufmann et al., 1984; Farmer and DePaolo, 1987, 1997; Eastoe and Guilbert, 1992). Variations in isotope ratios may act as tracers of chemical reactions, and can be sensitive to temperature, reaction kinetics, and fracture spacing (e.g., DePaolo, 2006). Perhaps the best example is the well-known shift in water oxygen isotopes as the ^{18}O depleted water exchanges with ^{18}O-enriched reservoir minerals (Craig et al., 1956; Magaritz and Taylor, 1976; Taylor, 1977). Changes in the dissolved Sr isotope composition driven by water–rock exchange along flow paths have been successfully modeled and applied as a tracer for mineral dissolution (e.g., Johnson and DePaolo, 1994; Jacobson and Wasserburg, 2005). Farmer and DePaolo (1987) found systematic variations in the Sr isotope ratios in alteration minerals in the hydrothermal halo around the San Manuel porphyry copper deposit, and used them to estimate the flow and reaction parameters that describe that hydrothermal system (Farmer and DePaolo, 1997).

Radiogenic isotope ratios like $^{87}Sr/^{86}Sr$ can offer temperature-independent estimates of water–rock reaction whereas other stable isotope systems like $^{44}Ca/^{40}Ca$ and $^{37}Cl/^{35}Cl$ are controlled by mass-dependent fractionation that can be both equilibrium (and temperature dependent) and kinetic. Changes in the radiogenic $^{87}Sr/^{86}Sr$ of fluids mainly reflect dissolution of minerals with isotopic compositions that are different from the fluid; Radiogenic Sr isotopes in fluids are not affected by precipitation from solution, whereas $^{44}Ca/^{40}Ca$ (as well as $^{18}O/^{16}O$, D/H and stable $^{88}Sr/^{86}Sr$) could be affected. Ca is a useful isotopic tracer for hydrothermal systems because Ca-bearing igneous minerals like plagioclase, amphibole, and clinopyroxene are susceptible to dissolution in hydrothermal fluids, and secondary precipitate minerals (e.g., epidote, calcite) also contain Ca. Calcite solubility is strongly affected by dissolved CO_2 concentrations, so fluid degassing can also generate calcite precipitation. Hence Ca isotopes can also be a tracer of fluid degassing. At low temperature mass dependent Ca-isotope fractionation driven by calcite precipitation is controlled by surface reaction kinetics (Lemarchand et al., 2004; Tang et al., 2008a; DePaolo, 2011). According to the theory described by DePaolo (2011) there is reason to suspect that kinetic Ca (and O) isotopic effects can occur at higher temperature as long as the net mineral growth rate is sufficiently fast (Brown et al., 2009, 2010).

Combining water major element chemistry with the isotopes of water, Sr and Ca and the concentration of dissolved gases, processes controlling the composition of hydrothermal fluids (mixing, dissolution, precipitation and vapor loss) can be identified and monitored along a fluid flow path. Our objective in this study is to apply this suite of tracers systematically to a relatively well-characterized hydrothermal system (Goff et al., 1991; Sorey et al., 1991; Hilton, 1996; Suemnicht et al., 2007), which provides access to numerous hydrothermal, monitoring and scientific wells, along the flow path (Fig. 1). Fluids from the wells were sampled for major ions, dissolved gases and the isotopes of water, Sr and Ca. For comparison, representative reservoir rocks and minerals were also analyzed for Sr and Ca isotope compositions.

2. GEOLOGIC BACKGROUND

The Long Valley caldera is a ~540 km^2 depression located on the border between the Sierra Nevada and Basin and Range physiographic provinces. The caldera formed following the eruption of the Bishop Tuff approximately 0.76 ma (Bailey et al., 1976; Sarna-Wojcicki et al., 2000). Subsequent volcanism included extensive rhyolite eruptions that closely followed the Bishop Tuff (0.75 ma) and formed a central dome, and then additional post caldera rhyolite and basalt in the west and south moat regions of the caldera at 0.5, 0.3 and 0.1 ma, and rhyodacite along the western rim at Mammoth Mountain at about 0.05 ma (Bailey et al., 1976; Hildreth, 1979, 2004; Mahood et al., 2010). The most recent activity is largely high-silica rhyolite erupted since about 18 ka along the Mono-Inyo chain (Hildreth, 2004). The present phase of geothermal activity in Long Valley has been active for the last 30–40 ka based on tufa deposits and hydrothermally altered sediments (Flexser, 1991; Sorey et al., 1991; Hurwitz et al., 2010).

Meteoric recharge of the hydrothermal system is thought to occur in the northwestern rim of the caldera, likely along the caldera ring fracture (White et al., 1990). The highest temperature hydrothermal fluid samples were collected from well RDO-8 and Unocal 44-16 (Fig. 1). Sorey et al. (1991) suggest that the region where hydrothermal fluids up-well from depth is west of RDO-8 and likely south of 44-16 based on potentiometric surfaces and fluid temperatures. Once hydrothermal fluids enter the uppermost Bishop Tuff and lower post caldera rhyolites they are thought to flow laterally from northwest to southeast (Fig. 1; Goff et al., 1991; Sorey et al., 1991).

Extensive studies of drill cores into the hydrothermal reservoir have characterized the secondary mineralogy that includes clays (kaolinite, smectite and illite), quartz, sulfides and calcite (Flexser, 1991; Goff et al., 1991; White and Peterson, 1991; McConnell et al., 1997). The clay mineralogy in the west moat drill cores is broadly consistent with hydrothermal fluids near or above 200 °C, similar to present-day fluid temperatures (Flexser, 1991). Previous sampling of hydrothermal fluids from the west moat and the Casa Diablo are saturated with quartz, calcite and pyrite, consistent with observed secondary minerals in drill cores (Flexser, 1991; White and Peterson, 1991).

3. METHODS

Hydrothermal fluids were sampled using two distinct techniques. Liquid water samples from the production wells feeding the Casa Diablo geothermal plant were collected from sampling ports on the wellhead and are identified in

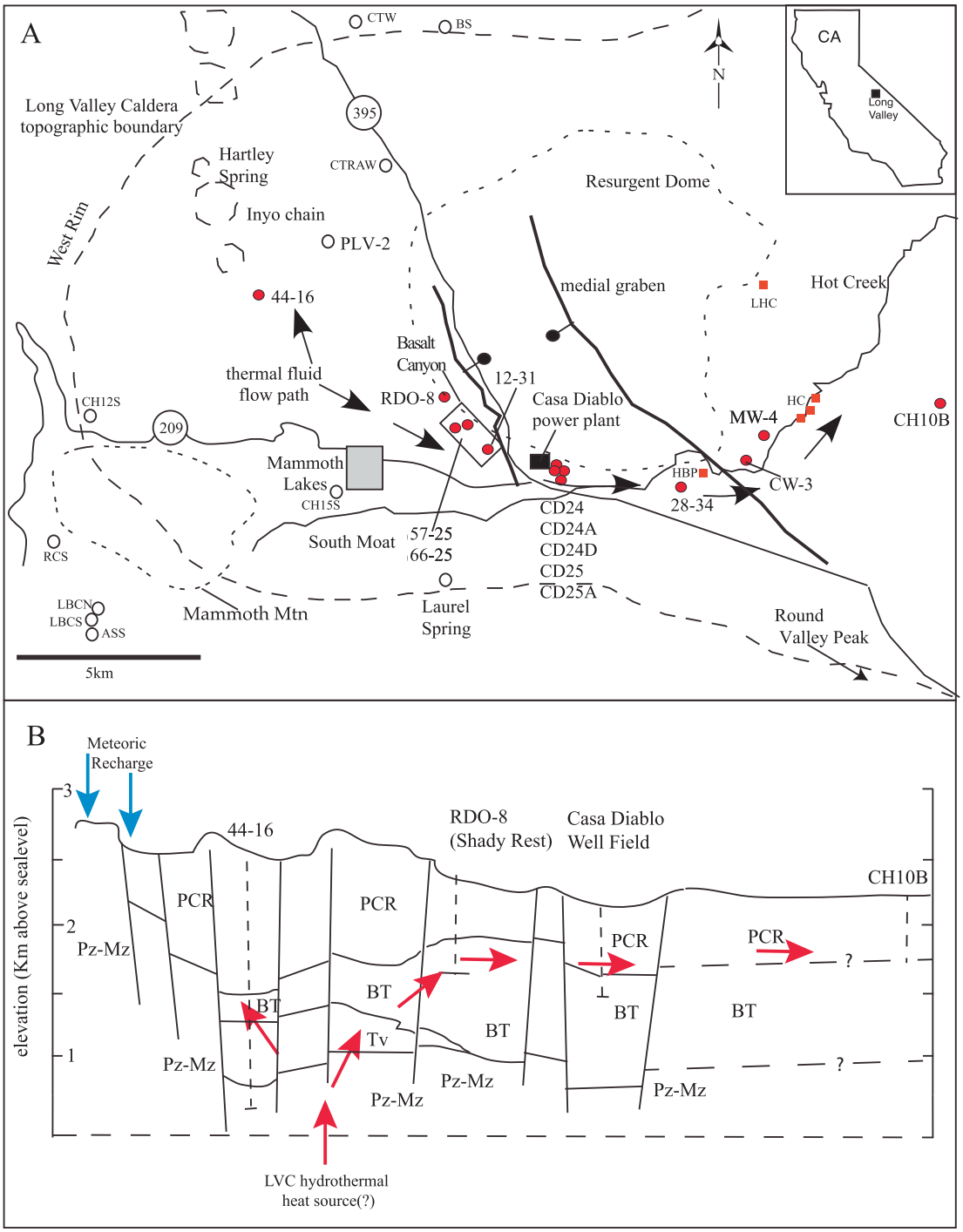

Fig. 1. (A) Map of study area after (Bergfeld et al., 2006). Thermal water samples collected from wells are noted with filled circles. Other thermal features are shown as filled squares. Cold spring, well and surface water samples are noted with open circles. Sample abbreviations are from Table 4 and (Evans et al., 2002). The proposed fluid flow path is shown with sub-horizontal black arrows. The topographic boundaries for the caldera and resurgent dome are shown as dashed lines. (B) Schematic cross section along the proposed hydrothermal flow path with the depths of research wells for reference. Lithologic contacts are adapted from Sorey et al. (1991) and Goff et al. (1991). Lithologic units are: Bishop Tuff (BT), Tertiary Volcanics (Tv), Post Caldera Rhyolites (PCR) and Paleozoic metamorphics (Pz-Mz).

the data tables by the sampling depth "wellhead". Fluid samples collected from wells east and west of the production field were collected using either a Kuster© down-hole sampling device (Kuster Company, Long Beach, CA, USA) or a bladder pump. Both techniques allowed for dissolved gases including CO_2 to be extracted at downhole

Table 1
Ca and Sr isotope compositions of Long Valley Basement Lithologies.

Lab ID	Sample ID	Sample description	$^{87}Sr/^{86}Sr$	2σ	$\delta^{44/40}Ca$	2σ	Ca wt%	Sr mg/g	Log D_{Sr}[a]	$\Delta^{44/40}Ca$[c]
	Mt. Morrison Metamorphic									
MM50	CL30Q	Mt. Morrison Hfs-S 58% Wo	0.715351	±25	−0.32	0.01	16.3	48	–	
MM51	CL20G	Mt. Morrison SS 19% CC	0.721402	±18	−0.09	0.25	7.8	65	–	
MM52	CL20L	Mt. Morrison SS	0.713473	±10	−0.56	0.08	0.3	6	–	
MM54	CL20I	Mt. Morrison M	0.707518	±36	−0.40	0.06	15.2	441	–	
MM55	CL30 N	Mt. Morrison Hfs-S 37% Wo	0.717058	±7	−0.36	0.06	1.2	9	–	
	Igneous									
MM53	CL9C	Round Valley Peak Granodiorite	0.709059	±6	−0.10		3.49	462	–	
	92DLV-113[b]	Inyo Domes Rhyolite	0.70611		0.11	0.2				
	Secondary Carbonates									
57-25 cc	57-25 cc	Secondary CC precipitated in well casing	0.707941	±3	−0.70	0.1		12,748	−0.09	−0.55
1191 cc	1191 cc	Secondary CC sampled at 1191 ft below ground surface from RDO-8 drill core	0.708754	±17	−0.52			3305	−0.79	−0.37
1204 cc	1204 cc	Secondary CC sampled at 1204 ft below ground surface from RDO-8 drill core	0.708705	±6	−0.53			4155	−0.69	−0.38
1844 cc	1844 cc	Secondary CC sampled at 1844 ft below ground surface from RDO-8 drill core	0.707807	±19	−0.25			1171	−1.24	−0.10

Sample IDs starting with CL are from Ferry et al., 2001. The remaining samples are secondary carbonates described in the text. Sample lithology is noted as sandstone (SS), Hornfels with sandstone protolith (Hfs-S), and Marl (M). The dominant Ca bearing phase calcite (CC) and wollastonite (Wo) and its modal abundance is noted where available. Ca isotope compositions are averages of 2 or more replicate analyses and the errors are 2 standard devations of the mean.

[a] $D_{Sr} = Sr/Ca_{calcite}/Sr/Ca_{fluid}$.

[b] Ca and Sr data from DePaolo (2004).

[c] $\Delta^{44}Ca$ for calcites is $= 1000LN(R_{prod}/R_{react})$ where R_{prod} and R_{react} are the isotopic ratios of the calcite and reactant pool at any given instant. $D^{44}Ca$ also assumes that the composition of the measured fluids are invariant with respect to time.

conditions. For the Kuster and bladder pump samples the strategy was to collect from a depth representing the highest temperature in the well (Table 1). Temperature, alkalinity and pH were determined in the field for at least one sample from each well. Samples for cation concentrations, Ca, and Sr isotopes were collected in acid cleaned HDPE bottles, filtered and acidified to pH ≈ 2 prior to laboratory work, while separate, filtered, un-acidified fluid aliquots were reserved for anion and water isotopes determinations.

Samples from Mt. Morrison sandstones, metasandstones and marls and the Round Peak Granodiorite, similar to the assumed basement lithologies, were analyzed for the isotopes and concentrations of Sr and Ca. The collection and petrology of the Mt. Morrison and Round Peak samples is detailed elsewhere (Ferry et al., 2001). Carbonate samples from well RDO-8 were collected from core stored at the Energy and Geothermal Institute at the University of Utah. The carbonate sample from well 57-25 was sampled from an extracted well casing.

Chemical and isotopic analyses were carried out using well-established techniques at UC Berkeley, Lawrence Berkeley National Lab, and the USGS (e.g., Evans et al., 1981, 1988; Fantle and DePaolo, 2006; Révész et al., 2008a,b; Nielsen et al., 2011). Specific methods used for this study are described in the supplemental methods section.

Isotope ratios of Ca, O and H are reported in the common delta notation where:

$$\delta^{44/40}Ca = \left(\frac{\frac{44}{40}Ca_{sample}}{\frac{44}{40}Ca_{BSE}} - 1\right) * 1000$$

Bulk Silicate Earth has $^{44}Ca/^{40}Ca = 0.212035$ assuming $^{42}Ca/^{44}Ca = 0.31221$ (Caro et al., 2010; Simon and DePaolo, 2010). The commonly measured SRM915a standard yields −1.0‰ on the BSE scale.

$$\delta^{18/16}O = \left(\frac{\frac{18}{16}O_{sample}}{\frac{18}{16}O_{SMOW}} - 1\right) * 1000$$

$$\delta^{\frac{2}{1}}H = \left(\frac{\frac{2}{1}H_{sample}}{\frac{2}{1}H_{SMOW}} - 1\right) * 1000$$

Radiogenic Sr is reported as the ratio of $^{87}Sr/^{86}Sr$ and corrected for instrumental mass fractionation using $^{86}Sr/^{88}Sr = 0.1194$. Fractionation factors are expressed as $\Delta^{44/40}Ca$ where:

$$\Delta^{\frac{44}{40}}Ca \approx 1000 \ln(R_{cal}/R_{aq}) \quad (1)$$

R_{cal} and R_{aq} are the $^{44}Ca/^{40}Ca$ ratios of the calcite and aqueous dissolved Ca respectively at any instant. The distribution of Sr between the hydrothermal fluid and calcite for given calcite samples is quantified as K_{Sr} using the equation:

$$K_{Sr} = \frac{\frac{Sr}{Ca}cal}{\frac{Sr}{Ca}aq} \quad (2)$$

The primary assumption in the calculated fractionation factors and distribution coefficients is that measured fluid samples from RDO-8 and 57-25 are representative of fluids from which the calcite precipitated (Table 1).

4. RESULTS

In this section we summarize the observations that allow us to use Ca isotopic compositions of Long Valley fluids and hydrothermal minerals to gain information about the processes that affect fluid evolution during passage through the system. The interpretation of the isotopic data starts with characterization of the compositions of major host rock lithologies and fluid sources. We then use the measurements on hydrothermal minerals and fluids to develop estimates for fluid-mineral reaction rates, fracture spacing in the active hydrothermal system, and calcite precipitation rates, and also provide evidence that calcite precipitation is kinetically controlled at hydrothermal conditions.

4.1. Host rock isotopic compositions

The Ca isotopic compositions of igneous and metamorphic rocks and hydrothermal calcites collected from Long Valley are presented in Table 1 and Fig. 2. Samples of igneous rocks reported here (Round Peak Granodiorite and Inyo Domes Rhyolite) and in the literature define a narrow range of δ^{44}Ca (±0.1‰) that indistinguishable from the value for bulk silicate Earth (Skulan et al., 1997; Simon and DePaolo, 2010). This indicates that the complex processes that produce granitic rocks result in minimal fractionation of Ca isotopes. The Devonian meta-sedimentary sandstones and marls exposed at Mt. Morrison, within the southeast margin of the caldera, have δ^{44}Ca as low as −0.55‰, which is significantly different from the igneous lithologies, and similar to Paleozoic, Mesozoic, and early Cenozoic limestones reported in the literature (Fantle and DePaolo, 2007; Farkus et al., 2007; Table 1). The difference between the marine sediments and the igneous values is well documented in the literature but not fully understood; fractionation during weathering processes may be partly responsible. Lithologies similar to those exposed at Mt. Morrison are found beneath the resurgent dome and in landslide debris within the west moat Bishop Tuff deposits (Suemnicht, 1987; McConnell et al., 1997; Suemnicht et al., 2007).

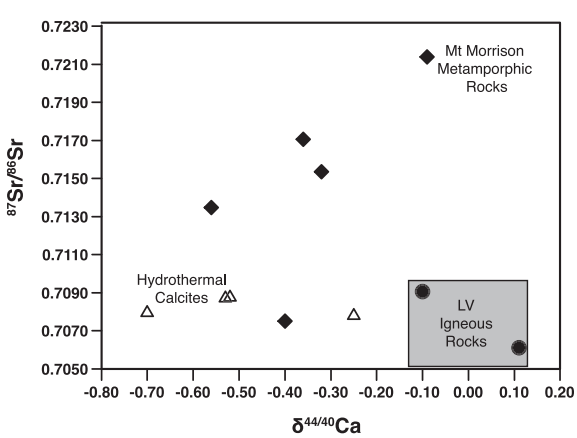

Fig. 2. The Sr-Ca isotope composition of rocks and secondary calcites from Long Valley. Mt. Morrison metamorphic rocks have correlated $\delta^{44/40}$Ca and ^{87}Sr/^{86}Sr, excluding the marl. The igneous rocks and secondary calcites have similar ^{87}Sr/^{86}Sr but the calcites are offset to lower $\delta^{44/40}$Ca.

The Sr isotopic compositions of Bishop Tuff and associated volcanic and metamorphic rocks have been reported elsewhere (e.g., Goff et al., 1991; Christensen and DePaolo, 1993). The Bishop Tuff has ^{87}Sr/^{86}Sr ~0.7060–0.7065 with some mineral phases and glass having values up to 0.7080–0.7085 (Christensen and DePaolo, 1993). Metamorphic rocks with sedimentary protoliths, such as the Mt. Morrison sandstones, exposed adjacent to the Long Valley caldera have ^{87}Sr/^{86}Sr of 0.7150–0.7250, while the Mt. Baldwin marble and wollastonite samples from Mt. Morrison have values of 0.7075–0.7080 (Goff et al., 1991; Table 1; Fig. 2). Igneous lithologies from the Sierra Nevada batholith typically have ^{87}Sr/^{86}Sr 0.706–0.708 (Kistler and Peterman, 1973; Kistler et al., 1986). The δ^{18}O of the igneous rocks is typically in the range +7 to +10 (Masi et al., 1981), limestones are ca. +20 to +30, and meta-sandstones are in the range +12 to +20 (Ferry et al., 2001; Lackey and Valley, 2004). The Bishop Tuff and related rhyolites have δ^{18}O values of +6 to +10 (e.g., Halliday et al., 1984). Overall, the δ^{18}O values of all of the rocks are high relative to the values in the fluids, which are mostly close to −15. This large contrast means that dissolution of minerals into fluid can tend to increase the δ^{18}O of the fluids, and exchange of oxygen between fluids and rocks tends to lower the δ^{18}O of the rocks (Taylor, 1974) (See Table 2).

4.2. Hydrothermal fluid chemistry

Water samples collected from wells along a ~14 km transect of the mostly horizontal hydrothermal flow path have moderate pH (5.5–6.7) chloride concentrations <300 ppm and temperatures between 220 and 100 °C (Fig. 3). Fluid temperatures, boron (B) and chloride (Cl^-) concentrations are highest in the West Moat well 44-16 and decrease eastward in the direction of flow (Fig. 3). Deuterium/hydrogen ratios (expressed as δD) are also highest in the West Moat but show less systematic west to east variation. We consider the sample from well 44-16 to be an end-member hydrothermal fluid, representative of the fluid upwelling from depth and constituting the starting composition from which we can measure changes along the west-to-east flow path. Based on several chemical and isotopic parameters the well 44-16 sample is the least affected by meteoric water addition, vapor loss, and mineral precipitation; the processes that appear to be responsible for the fluid chemical evolution along the flow path. Our sample does not show the anomalously high Na and SO_4 found in a 1986 sample from this well and attributed by Sorey et al. (1991) to contamination by drilling fluid. Presumably, the drilling fluid has been flushed from the well during the 20 intervening years. Although fluid flow directly from the location of well 44-16 to the rest of the study area is unlikely, in our view the sample from 44-16 represents the best estimate we have for the composition of the deeper hydrothermal fluids feeding the shallow lateral flow zone in Long Valley.

The concentrations of Sr and dissolved CO_2 decrease eastward along the flow path (Fig. 3). The fluid sample

Table 2
Long Valley fluid sample descriptions and selected chemistry.

Well ID/map abbrevation	Sample collection date	Km from 44-16	Temp (°C)	Alkalinity (mg/L)	pH (field)	pH (calc)	Ca (μg/g)	Sr (ng/g)	Cl (ug/g)	CO_2 (mmol/Kg)	% meteoric water
Production and monitoring wells											
West Moat											
44–16	6/27/2005	0.00	190	414	5.7	6.3	19.8	395	286	59.0	0
PLV-2	6/30/2005	–	42	481	6.7	–	16.8	71.9	29.4	5.80	91.0
RDO-8	7/18/2007	5.48	–	488	–	6.8	5.92	330	273	25.0	4.5
Basalt Canyon											
12–31	6/29/2005	7.34	184	572	6.5	–	7.05	364	149	18.6	48.6
CD57-25	10/1/2006	6.37	170	553	5.9	–	5.73	224	255	37.8	11.0
	6/28/2007	6.37	170	–	–	–	–	–	234	–	18.4
CD66-25	10/1/2006	6.63	170	520	6.1	–	3.81	182	251	16.5	12.4
	6/28/2007	6.63	170	–	–	–	–	–	254	–	11.3
Casa Diablo Well Field											
CD24	10/1/2006	9.17	150	479	6.5	6.9	2.90	166	240	5.00	16.5
CD24A	6/28/2005	9.32	150	475	6.4	–	–	145	237	–	17.4
	9/30/2005	9.32	150	–	–	–	–	139	233	–	–
	10/1/2006	9.32	150	–	–	–	–	147	–	–	–
	6/28/2007	9.28	150	–	–	–	–	139	–	–	–
CD24D	6/28/2005	9.28	150	–	–	–	–	150	222	–	22.7
	9/30/2005	9.28	150	–	–	–	–	160	–	–	–
CD25	10/1/2006	9.28	150	468	6.4	–	–	130	238	–	17.0
	6/28/2007	9.28	150	–	–	–	–		–	–	–
CD25A	7/1/2005	9.36	150	–	–	–	–	115	238	–	17.0
	9/30/2005	9.36	150	–	–	–	–	139	–	–	–
	6/28/2007	9.36	150	–	–	–	–	–	–	–	–
Eastern Caldera Wells											
28–34	6/28/2005	12.53	150	404	6.4	6.6	6.32	68.0	198	7.77	31.2
CW-3	7/13/2007	13.96		426	6.4	6.6	6.00		202	–	29.8
MW4	7/13/2007	–	–	–	–	–	–	–	4.0	–	100
CH10B	7/13/2007	14.48	100	497	7.0	7.1	16.7	323	157	0.540	45.7
Hot Springs											
BAL	8/12/1998	–	57	778	6.7	–	–	192	148	–	48.9
LHC	8/12/1998	–	79	734	6.8	–	–	598	200	–	30.5
HBP	8/12/1998	–	79	444	7.5	–	–	121	217	–	24.5
Cold springs, wells and surface waters											
BS	8/11/1998	–	*12.3*	*2.1*	*7.23*	–	*6.2*	65	*5*	*0.3*	–
CTRAW	8/11/1998	–	*13.8*	*2.5*	–	–	*6*	45	*2.5*	–	–
CTW-2	8/11/1998	–	*17.6*	*1.2*	*8.46*	–	*9.2*	106	*4.2*	*0.01*	–
CH12S	8/11/1998	–	*2.4*	*1.5*	*5.07*	–	*19.2*	103	*0.28*	*43.3*	–
RMCS	8/13/1998	–	*7.4*	*2.5*	*5.41*	–	–	112	*0.28*	*28.7*	–
ASS	8/13/1998	–	*6.2*	*2.0*	*5.48*	–	13.6	116	*0.27*	*20.2*	–
LBCS	8/13/1998	–	*7.2*	*2.3*	*5.43*	–	14.9	124	*0.4*	*25.8*	–
LBCN	8/13/1998	–	*6.8*	*2.6*	*5.49*	–	17.1	144	*0.45*	*25.4*	–
LS	8/13/1998	–	–	–	–	–	–	32	–	–	–

Fraction meteoric water calculated from Cl^- concentrations assuming 286 ppm in the hydrothermal endmember and 4 ppm in the meteoric endmember using mixing equations of Langmuir et al., 1978. Data in italics was previously presented in Evans et al. (2002).

from well 44-16 has 60 mmol/kg-dissolved gases, 98% of which is CO_2. The apparent eastward rate of CO_2 decrease is large between 44-16 and RDO-8 (~11 mmol kg^{-1} km^{-1}), and smaller (~6 mmol kg^{-1} km^{-1}) in the main Casa Diablo well field. Calcium concentrations also decrease systematically eastward from well 44-16 to the Casa Diablo region, and then increase east of Casa Diablo by a factor of 2–4 while CO_2 concentrations remain low in the easternmost portion of the hydrothermal system (well CH10B; Fig. 2). Alkalinity (HCO_3^-) increases from 414 mg/L in well 44-16 to >520 mg/L in the Basalt Canyon wells (57-25 and 66-25) and then decreases to 404 mg/L in well 28-34, then increasing to 497 mg/L in well (CH10B; Fig. 3). The ratios of Sr/Ca (not shown) and $^{44}Ca/^{40}Ca$ increase from well 44-16 to Casa Diablo and decrease east of the well field (Fig. 3).

The $^{87}Sr/^{86}Sr$ of the hydrothermal fluids increases from well 44-16 to the Basalt Canyon wells (57-25 and 66-25).

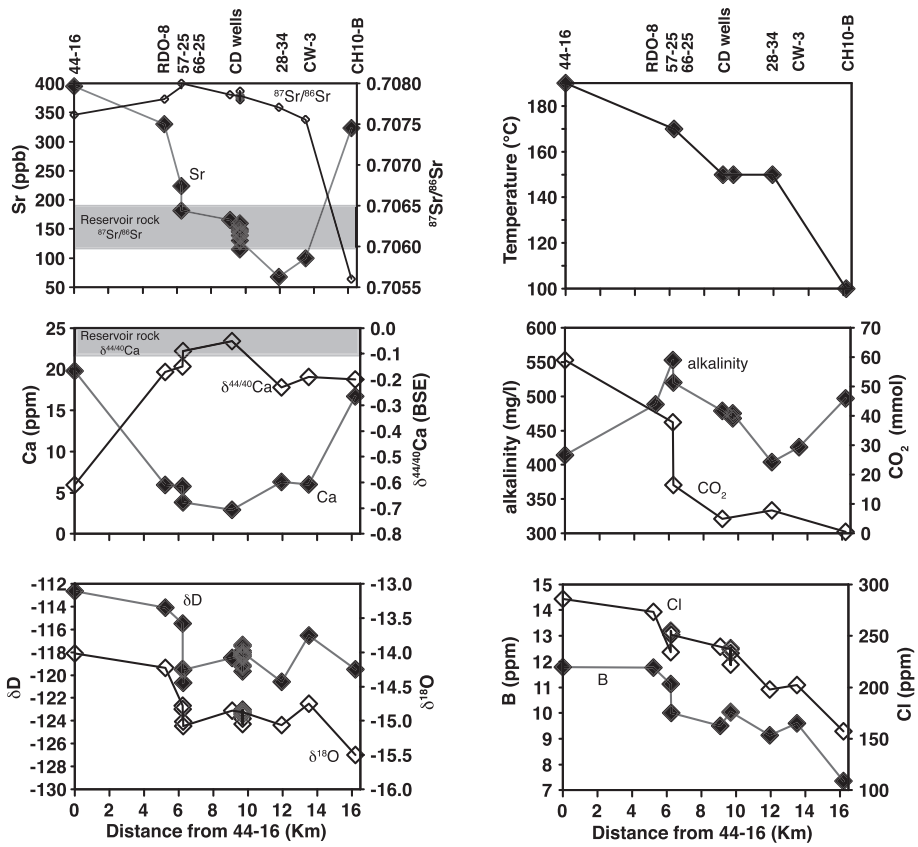

Fig. 3. Temperature and chemistry variations in Long Valley hydrothermal fluids along the proposed flow path. Only samples from production, monitoring and research wells are shown. Temperatures are the maximum measured fluid temperature for each well.

East of Basalt Canyon there is a trend of declining $^{87}Sr/^{86}Sr$ along the flow path to CW-3. All hydrothermal fluid samples have higher $^{87}Sr/^{86}Sr$ than Bishop Tuff (0.7060–0.7065) with the exception of CH10B (0.7056), which has the least radiogenic Sr of any fluid sample within the caldera. The high $^{87}Sr/^{86}Sr$ measured in BC12-31 and MW4 are thought to reflect contamination with drilling mud and/or water as evident from other chemical anomalies encountered in these wells (Fig. 3).

Our water isotope data (Table 3) show considerably less scatter than data reported earlier (White et al., 1990; Sorey et al., 1991; Fig. 4), probably due to improved sampling and analytical techniques. The equation of the best fit line through the hydrothermal fluid data is $\delta D = 5.8\ \delta^{18}O$. The slope of 5.8 is significantly lower than the standard meteoric water line slope of 8 and is typical of many hydrothermal systems (Craig, 1961). Water samples from wells RDO-8 and 44-16 (White et al., 1990; Table 3); have the highest $\delta^{18}O$ (−14.0 to 14.2). Sample MW-4 has the lowest value and falls close to the meteoric water line at $\delta^{18}O = -18.0$. A large fraction of the samples from the southwest moat cluster in a fairly tight range of $\delta^{18}O$ between −14.6 and −15.2 and δD, between −116 and −122. This cluster includes almost all of the samples along the flow path transect from RDO-8 to CW-3. These data suggest that in this region of the hydrothermal system there is a single hydrothermal fluid that does not evolve in water isotopic composition as it traverses 8 km laterally from west to east. The $\delta^{18}O$ of this fluid is distinct from local meteoric water, but also greatly different from typical high temperature magmatic water, which has $\delta^{18}O$ of about +6 to +8 (Taylor, 1974; Fig. 3). Hence, as noted by (White et al., 1990) the dominant hydrothermal fluid must be a mixture between a hydrothermal fluid (high $\delta^{18}O$) and local meteoric water; the latter having $\delta D \approx -135$ and $\delta^{18}O \approx -18$ as inferred from a regression through the hydrothermal fluid data (Fig. 4).

Despite 30 years of drilling (e.g., Sorey et al., 1991; Suemnicht et al., 2007) and an extensive study of regional precipitation (White et al., 1990) no meteoric water with the inferred water isotope composition has been found in the western side of the caldera (Sorey et al., 1991). It has been suggested that the meteoric component may be an older (>1000 a) groundwater derived from precipitation during a time of colder climate (White et al., 1990) or far-traveled groundwater (Sorey et al., 1991). These explanations are not entirely satisfactory when viewed in light of the short lifetime of water in the system.

4.3. Secondary hydrothermal minerals

Secondary calcite from wells RDO-8 and 57-25 have lower $\delta^{44/40}Ca$ compared to fluid samples from the same wells (Tables 1 and 3). The secondary calcite from well 57-25 has $\delta^{44/40}Ca = -0.70$, 0.55‰ lower than the associated fluid sample. Two bladed calcite samples from RDO-

Table 3
Isotopic compositions of Long Valley fluids.

Well ID	Date	$^{87}Sr/^{86}Sr^{b}$	2σ	$\delta^{44/40}Ca$	2σ	$\delta^{18}O$	δD
44–16	6/27/2005	0.707616	±7	−0.61	±0.20	−14.0	−112.7
PLV-2	6/30/2005	0.707231	±8	0.17	±0.01	−15.6	−117.0
RDO-8	7/13/2007	0.707809	±10	−0.17	±0.08	−14.2	−114.1
12–31	6/29/2005	0.708543	±10	−0.37	±0.30	−15.9	−123.0
CD57-25	10/1/2006	0.707939	±10	−0.15	±0.06	−14.8	−119.4
CD57-25	6/28/2007	0.707956	±18	–	–	−14.8	−115.5
CD66-25	10/1/2006	0.707998	±38	−0.09	±0.04	−15.1	−119.5
CD66-25	6/28/2007	0.708000	±11	–	–	−15.0	−120.7
CD24	10/1/2006	0.707863	±8	−0.05	±0.09	−14.9	−118.5
CD24A	6/28/2005	–	–	–	–	−14.9	−118.2
CD24A	9/30/2005	0.707825	±8	–	–	−14.9	−117.5
CD24A	10/1/2006	0.707825	±10	–	–	−14.9	−118.4
CD24A	6/28/2007	0.707850	±10	–	–	−14.8	−119.3
CD24D	6/28/2005	0.707804	±10	–	–	−14.9	−117.9
CD24D	9/30/2005	0.707803	±7	–	–	−15.1	−118.0
CD25	10/1/2006	0.707847	±10	–	–	−14.9	−118.0
CD25	6/28/2007	0.707846	±10	–	–	−14.9	−119.7
CD25A	7/1/2005	0.707845	±10	–	–	−15.0	−119.1
CD25A	9/30/2005	0.707903	±14	–	–	−14.9	−117.4
CD25A	6/28/2007	0.707846	±17	–	–	−14.9	−118.3
28–34	6/28/2005	0.707703	±10	−0.23	±0.08	−15.1	−120.6
CW-3	7/13/2007	0.707555	±8	−0.19	±0.10	−14.6	−116.5
MW4	7/13/2007	0.708217	±25	–	–	−18.0	−136.6
CH10B	7/13/2007	0.705600	±8	−0.2	±0.23	−15.5	−119.5
BAL	8/12/1998	0.707809	±17	–	–	–	–
LHC	8/12/1998	0.707793	±8	–	–	–	–
HBP	8/12/1998	0.707581	±13	–	–	–	–
BS	8/11/1998	0.706706	±16	–	–	*−115.3*	*−15.8*
CTRAW	8/11/1998	0.706495	±10	–	–	*−111.8*	*−15.7*
CTW-2	8/11/1998	0.706887	±25	–	–	*−122.9*	*−16.6*
CH12S	8/11/1998	0.706987	±10	–	–	–	–
RMCS	8/13/1998	0.706538	±8	–	–	*−107.3*	*−14.9*
ASS	8/13/1998	0.706867	±10	–	–	–	–
LBCS	8/13/1998	0.706716	±10	–	–	*−105.2*	*−14.7*
LBCS-N	8/13/1998	0.706659	±10	–	–	*−104.7*	*−14.7*
LS	8/13/1998	0.711931	±10	–	–	–	–

Data in italics were previously presented in Evans et al. (2002). $^{87}Sr/^{86}Sr$ are corrected for mass discrimination using $^{86}Sr/^{88}Sr = 0.1194$. The average value for NBS987 on the Berkeley Triton is 0.71025 ± 1. Ca isotope data is relative to bulk earth (BSE) as defined by Simon and DePaolo (2010). The average value for SRM 915A during this study was -0.97 ± 0.1.

8 (1204 and 1191ft below ground surface) also have low $\delta^{44/40}Ca = -0.52$ and -0.53, respectively. A massive calcite sampled from 1844 ft, in contrast, has $\delta^{44/40}Ca = -0.24$, similar to the RDO-8 fluid sample. The RDO-8 fluid sample was collected from a depth of 594 m (1950 ft).

The RDO-8 calcites have $^{87}Sr/^{86}Sr$ values 0.7075–0.7085 that are correlated with sampling depth and fluid temperature (Table 1; Goff et al., 1991). Carbonate scale sampled from well 57-25 has $^{87}Sr/^{86}Sr = 0.70800$, similar to the hydrothermal fluid sample 0.70796 (Table 3). The $^{87}Sr/^{86}Sr$ data are suggestive that the calcite scale samples precipitated from fluid that is similar to that sampled, but are fractionated in both $^{44}Ca/^{40}Ca$ and Sr/Ca relative to that fluid (Table 1).

4.4. Cold springs and stream chemistry

The locations and chemistry of cold spring, groundwater and surface water samples are presented in Fig. 1 and Table 4. The Ca concentrations in non-thermal water samples varies from 2.6 ppm at Hartley Spring to 49 ppm in the Chair 15 Spring on Mammoth Mountain (http://wwwrcamnl.wr.usgs.gov/volcwater/). Sr concentrations range from 3.8 ppm in the upper soda spring to as low as 15 ppb in Lake Mamie on Mammoth Mountain. Despite the large range in elemental concentrations, most of the non-thermal water samples have $^{87}Sr/^{86}Sr$ between 0.7070 and 0.7065 (e.g., Table 3), consistent with the range of $^{87}Sr/^{86}Sr$ of igneous rocks sampled in the immediate region (0.7060–0.7070; Goff et al., 1991; Christensen and DePaolo, 1993). One notable exception is Laurel Spring, where the spring water has $^{87}Sr/^{86}Sr = 0.7120$. Laurel Spring discharges on the south edge of the caldera from Paleozoic metamorphic rocks, which typically have higher $^{87}Sr/^{86}Sr$ than granitic rocks.

The only Ca isotope measurement that can help constrain the isotopic composition of the cold groundwater component is from PLV-2, a monitoring well located in the western portion of the caldera. A water sample from a depth of 555 m (1820 ft) has a temperature of 40 °C

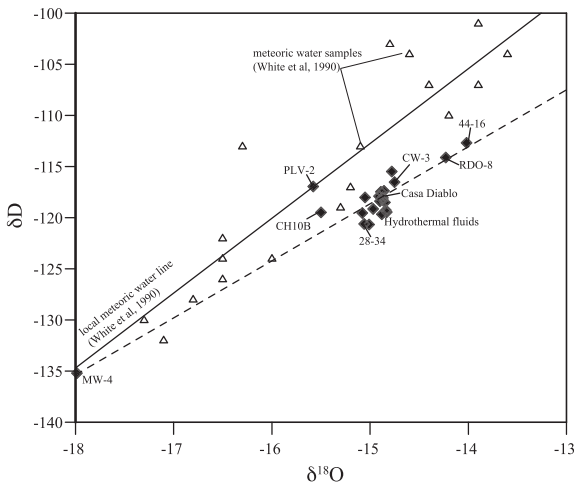

Fig. 4. Water isotopic compositions for hydrothermal fluids and meteoric water in Long Valley Caldera. Hydrothermal fluids are enriched in ^{18}O consistent with fluid rock isotope exchange in the deep reservoir. Convergence of the hydrothermal fluid trend with the meteoric trend is consistent with two-component mixing between the two fluids.

Table 4
Saturation index for Ca bearing minerals in select samples.[a]

Sample ID	$SI_{calcite}$	$SI_{anhydrite}$	$SI_{fluorite}$
44-16	0.734	0.163	0.054
RDO-8	0.457	−2.961	−0.207
CD57-25	0.045	−1.008	−0.531
CD66-25	−0.013	−1.28	−0.419
CD24-32	0.024	−1.49	−0.693
28-34	−0.288	−1.56	−0.311
CW3	−0.426	−1.88	−0.218
CH10B	0.205	−2.05	−0.275

[a] Saturation index = $\log_{10}$(IAP/K) calculated using SOLMINEQ (Kharaka et al., 1988). Uncertainty of saturation calculation is estimated to be 0.1.

and has low $\delta^{18}O$, properties that are similar to cold groundwater and meteoric water and different from hydrothermal fluid. The PLV-2 fluid has 16.8 ppm Ca and $\delta^{44}Ca = 0.23$, which suggests that non-thermal waters in LVC have $\delta^{44}Ca$ similar to local igneous rocks (−0.1 to +0.1; Fig. 2, Table 1). The $\delta^{44}Ca$ of low temperature waters will increase if they are affected by precipitation of calcite.

5. APPROACHES TO MODELING ISOTOPE VARIATIONS IN FLUIDS

Four complementary modeling approaches are employed in order to interpret the chemical and isotopic composition of LV hydrothermal fluids and secondary minerals. Mass balance equations, detailed extensively elsewhere (e.g., Langmuir et al., 1978), are employed to quantify mixing between thermal fluids and meteoric water. We then use relatively simple reactive transport models to produce estimates of dissolution and precipitations rates and fracture spacing. The thermodynamic code SOLMINEQ (Kharaka et al., 1988) is used to reconstruct fluid compositions at reservoir conditions and perform mineral solubility calculations. Our strategy is to use the measured cation, anion and gas compositions of the fluids to reconstruct the fluid composition at reservoir conditions. Importantly, the CO_2 concentrations coupled with on-site alkalinity titrations enable us to calculate the fluid pH at reservoir conditions. Chemical data used in the solubility calculations are summarized in the electronic appendix.

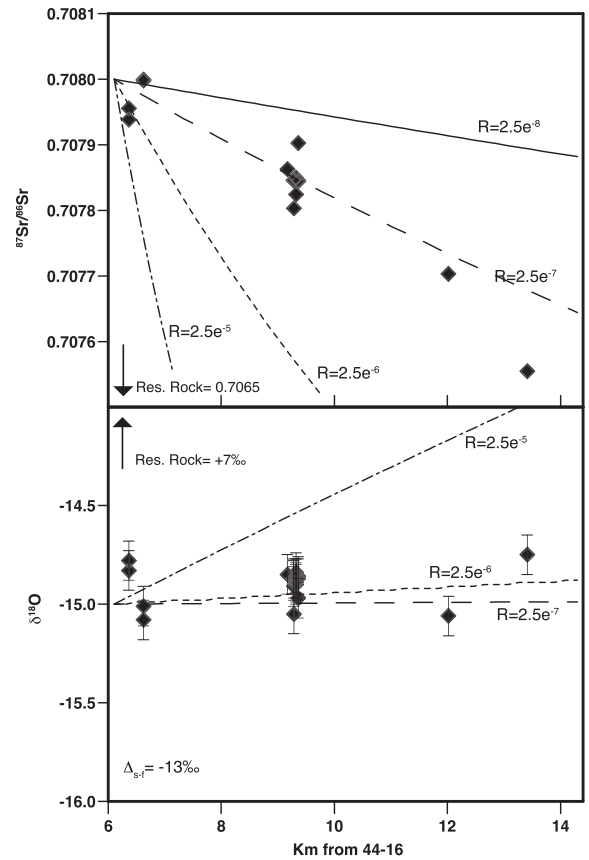

Fig. 5. Modeled and observed behavior of (a) Sr and (b) oxygen isotopes for a subsection of the LVC hydrothermal fluid flow path. Reaction curves were calculated with $K_{Sr} = 500$, $K_O = 0.55$, $D_{Sr} = 0.001$ $D_O = 0.07$, $b = 10$ m, $d = 0.25$ mm, $\varphi = 0.1$ and reaction time constants labeled on the figure. All variables are as defined in DePaolo (2006). The CW-3 O isotope value is adjusted by 0.2‰ consistent with the offset between the Berkeley and USGS data. All other O isotope values are as measured at Berkeley.

An analytical fracture flow model (DePaolo, 2006) is used to evaluate the isotopic evolution of fluid compositions due to water–rock reaction. The full model development and equations are presented in DePaolo (2006) and only the relevant portions are included here. The model consists of two components: the advective transport of fluid in fractures and diffusive transport of pore fluids from the rock matrix to the fractures. The model assumes that fluid-rock chemical exchange occurs in the rock matrix and the altered fluid is transported to fractures primarily by diffusion. An important assumption of this model is that the LVC system is at or near the steady-state condition, which will be further examined in Section 6.

The change in the elemental concentration or isotope composition of pore fluids C_f (mol/L^3) in a advective-reactive-dispersive system is a function of position and time and depends on velocity v (m y^{-1}), the ratio of the constituent in the water compared to the rock K, diffusivity (or dispersivity) D (m^2 y^{-1}), the bulk reaction rate R (y^{-1}), concentration in the solid C_s (mol/L^3) and the ratios of density ρ and porosity ϕ between the fluid and rock. If there is no net change in porosity the change in an element or isotope can be expressed as:

$$\frac{\partial C_f}{\partial t} = D\frac{\partial^2 C_f}{\partial x^2} - v\frac{\partial C_f}{\partial x} + RM(C_s - KC_f) \quad (3)$$

where,

$$M = \frac{\rho_s(1-\phi)}{\rho_f} \quad (4)$$

(e.g., Richter and DePaolo, 1988; Maloszewski and Zuber, 1991; Sanford, 1997; Skelton et al., 1997; Fantle and DePaolo, 2007). The DePaolo (2006) model makes the simplifying assumption that transport in the fractures is purely advective, and transport in the rock matrix between the fractures is purely by diffusion normal to the fractures. The steady-state isotopic ratio of the advecting fluid in the fractures (r_f) is described by:

$$\frac{dr_f(x)}{dx} = \frac{8D\phi_m}{v_f\phi_f bd}[r_s(x) - \alpha r_f(x)]\sum_{n_{odd}}\left(1 + n^2\pi^2\frac{L^2}{b^2}\right)^{-1} \quad (5)$$

where D (m^2 y^{-1}) is the diffusion coefficient applicable to the stagnant pore fluid in the matrix, and r_s is the isotope ratio in the matrix rock, d (m) is the fracture aperture, ϕ_m is the porosity of the matrix, ϕ_f is the porosity of the fracture (or equivalent high permeability zone), v_f is the fluid velocity in the fractures, and b (m) is the fracture spacing. The parameter α is the isotopic fractionation factor, which is assumed to be unity for a radiogenic isotope ratio like $^{87}Sr/^{86}Sr$, but is different from unity for stable isotope systems like O, H, and Ca. From the first factor on the right hand side of Eq. (5) it is evident that the rate of change with distance of the isotope ratio in the fracture fluid is higher if the matrix diffusivity and porosity is higher, and lower if the velocity and fracture spacing is larger. The effect of reactions in the matrix between the fractures is captured largely in the dimensionless ratio L/b, which is a form of Damköhler number

$$L/b = \frac{2}{b}\left(\frac{D_1}{R_m MK_i}\right)^{1/2} \quad (6)$$

which relates the fracture spacing (b), to the diffusive reactive transport lengthscale that is determined by the rate of dissolution/precipitation in the matrix regions (R_m) and the fluid phase transport characteristics of the inter-fracture matrix (DePaolo, 2006). If $L/b << 1$, then the isotopes of the fluid flowing in the fractures equilibrate slowly with the main volume of rock in the matrix regions between the fractures, and fracture fluid differs markedly from the average matrix pore fluid. If the $L/b \geqslant 1$, then the isotopes of the fluid flowing in the fractures exchange more rapidly with the inter-fracture matrix, the flowing fracture fluid and the stagnant matrix fluid are similar in isotopic composition, and the system behavior approaches that of a homogeneous porous medium. Slow equilibration occurs when the fracture spacing (b) is large, when the rock reaction rate (R_m) is small, and when the rock/fluid mass balance for the element of interest (MK_i) is large.

Treatment of Ca isotopes in reactive transport models requires an additional consideration that has been recognized only recently. In most treatments of stable isotopes, it is assumed that the fractionation factor α is a function of temperature only. However, for calcium in particular, recent work has shown that most of the (small) fractionation is kinetic in origin and the fractionation factor is dependent on precipitation rate (DePaolo, 2011; Nielsen et al., 2012). The details of the models are not important for our purposes, rather the important point is the observation that calcite precipitated from aqueous solution at rates typical for laboratory experiments (10^{-8} to 10^{-6} mol/m^2/s) result in calcite with δ^{44}Ca that is about 0.5–1.5‰ lower than the dissolved Ca in solution (e.g., Tang et al., 2008a,b). In contrast, calcite precipitated close to equilibrium at the extremely slow rates typical of marine diagenesis ($<10^{-12}$ mol/m^2/s) has δ^{44}Ca that is virtually identical to that of the dissolved Ca in the pore fluids (e.g., Fantle and DePaolo, 2007). This relationship is captured approximately in the DePaolo (2011) model with the following equation, which assumes first order kinetics for the calcite precipitation reaction. The precipitation rate dependent fractionation factor (α_p) is given by:

$$\alpha_p = \left(\frac{r_{solid}}{r_{fluid}}\right)_{ss} = \frac{\alpha_f}{1 + \frac{K_{eq}}{Q}\left(\frac{\alpha_f}{\alpha_{eq}} - 1\right)} \quad (7)$$

where Q/K_{eq} gives the departure from equilibrium (oversaturation factor), α_{eq} is the equilibrium fractionation factor (applicable as $Q \rightarrow K_{eq}$) and α_f is the kinetic fractionation factor (applicable for $Q >> K_{eq}$). For the low-temperature experimental results available in the literature, there is significant kinetic fractionation (>0.5‰ in $\delta^{44/40}$Ca) when $Q \approx 2K_{eq}$ (2× oversaturation). Nielsen et al. (2012) show that Eq. (7) is not an accurate representation for α_p at low oversaturations, as noted also by DePaolo (2011).

6. DISCUSSION

6.1. Lateral evolution of hydrothermal fluids

Systematic variations in the elemental and isotopic compositions of hydrothermal fluids along the Long Valley lateral flow path are likely the result of multiple processes such as mixing, mineral dissolution-precipitation and degassing. Our strategy is to account for the effects of mixing on the Sr and Ca isotope compositions of the fluids and then quantify the respective roles of dissolution and precipitation, which in turn relate to fracture spacing and fluid velocity.

6.1.1. meteoric-thermal water mixing

Eastward flowing hydrothermal fluids are diluted with meteoric water that is characterized by relatively low δD (−137) and δ^{18}O (−18) and low Cl^- concentrations

(4 ppm; Figs 3 and 4, White et al., 1990). The meteoric end-member is defined based on the intersection of the hydrothermal fluid sample array with the local meteoric water line, which happens to be coincident with the composition of sample MW-4. We use Cl^- concentrations as a measure of the amount of meteoric water addition along the lateral flow path of hydrothermal fluids.

Mass balance models indicate that, excluding the easternmost sample CH10B, the hydrothermal fluid samples contain 0–30% additional meteoric water. If the meteoric water component has $\delta^{44/40}Ca$ of 0, similar to igneous rocks, then there is likely only a maximum 0.1–0.2 per mil shift in the fluid Ca isotope composition due to mixing. Moreover, the samples with the greatest fraction meteoric water, those from wells CW-3, 28–34 and CH10B, have low $\delta^{44/40}Ca$ (−0.19 to −0.23) compared to the Casa Diablo sample CD24 ($\delta^{44/40}Ca = -0.05$), opposite to the expected effect from addition of igneous-derived Ca associated with meteoric-hydrothermal fluid mixing (Fig. 3).

We estimate that the meteoric water component has between 10 and 50 ppb Sr based on the compiled USGS surface and groundwater data (http://wwwrcamnl.wr.usgs.gov/volcwater/). If the meteoric component contains 40 ppb Sr, for example, and has $^{87}Sr/^{86}Sr$ similar to the Bishop Tuff (0.7065) it can account for 20–30% of the observed isotopic shift in Sr between the Basalt Canyon wells 57-25 and 66-25 and the eastern caldera wells 28-34 and CW3. Since there is a relatively large uncertainty in the Sr concentration of the meteoric end member and the total effect of mixing appears small we have chosen to assume initially that the effects of meteoric fluid addition are negligible and then assess the effect on the conclusions if they are not.

6.1.2. Reservoir rock dissolution

The Basalt Canyon hydrothermal fluid samples have the most radiogenic Sr with less radiogenic Sr both west and east (Figs 3 and 5; Table 3). The apparent increase in $^{87}Sr/^{86}Sr$ between well 44-16 and Basalt Canyon may indicate that as the fluid traverses the western portion of the study area it is reacting with a more radiogenic lithology. This is supported by more radiogenic basement lithologies beneath and intermixed with the Bishop Tuff (Suemnicht, 1987; Suemnicht et al., 2007). Suemnicht et al. (2007) suggest that the landslide debris in the Bishop Tuff are critical to maintaining separation between the hydrothermal fluid and groundwater.

The hydrothermal reservoir segment that extends from the Basalt Canyon wells (57-25 and 66-25) to CW3, shows a systematic downward shift in $^{87}Sr/^{86}Sr$ that may yield information on the rate of dissolution reactions. The shift in $^{87}Sr/^{86}Sr$ between Basalt Canyon and CW-3 is relatively small (0.70800 to 0.70755) but well resolved. The fracture flow model from Eq. (5) is used to evaluate which sets of flow parameters are consistent with the observed shift in Sr isotopes and absence of change to the $\delta^{18}O$ of the hydrothermal fluids. For the Long Valley lateral flow system we know that the fracture fluid velocity is high (500–2000 m y^{-1}) based on isobutane arrival times downgradient from Casa Diablo (Evans et al., 2004). The remaining variables contained in Eq. (5) are the ionic diffusivity, distribution coefficient, density of the reservoir rock and fluid, and fracture aperture and spacing. We set the diffusivity of oxygen to 0.07 m^2 y^{-1} and Sr to 0.001 m^2 y^{-1}, the ratio of rock/fluid density to 2.6, the distribution coefficient (K) to 500 and matrix rock porosity to 10%. The fracture spacing and fracture aperture were initially set to 10 m and 0.1 cm, respectively. Evaluating Eq. (5) with the above parameters allows us to solve for the dissolution rate (R_m), which is constrained by the available data to be about 2.5×10^{-7} g (reservoir rock) g^{-1} (reservoir rock) yr^{-1} (Fig. 5). We also tested the sensitivity of the fracture spacing and determined that it is required to be large ($\geqslant$10 m) to allow for Sr isotope evolution in the absence of O isotope changes. These parameters result in a good fit to the Sr isotope data, and minimal shift in $\delta^{18}O$ as observed. The inferred rock dissolution or reaction rate is faster than typically observed for weathering reactions at surface conditions ($\leqslant 10^{-8}$ g g^{-1} yr^{-1}), but slower than rates estimated for regional metamorphic rocks at greenschist facies conditions (ca. 500 °C), which are closer to 10^{-6} g g^{-1} yr^{-1} (Baxter and DePaolo, 2000). Reaction rates can be much faster if the fluids are acidic (Ryu et al., 2011), but the LV fluids have near-neutral pH.

If the shift in $^{87}Sr/^{86}Sr$ with distance is due to mixing with a deep, high Sr concentration groundwater, then the calculated reaction rate is an artifact, and the actual reaction rate would need to be much lower. If a fraction of the Sr isotope shift is due to mixing, then the estimated reaction rate would need to be lowered by approximately that fraction. We consider the mixing model explanation to be unlikely because it does not explain the observed CO_2 concentrations. The high Sr concentration groundwater and cold springs in the LVC also have high CO_2 concentration (Evans et al., 2002). For example sample DCWELL2 of Evans et al. (2002) has >400 ppb Sr and 16 mmol/kg CO_2, higher concentrations than observed at Casa Diablo and the eastern monitoring wells. This implies that if a high Sr groundwater was mixing with the hydrothermal fluid there should be an increase in CO_2 and Sr concentrations eastward, opposite to what is observed. We conclude that the systematic eastward shift of Sr isotopes is unlikely to be caused purely by an admixture of meteoric water, although there could be a small contribution that would then result in slightly lower values for the estimated dissolution rates.

6.1.3. Inferences about reservoir characteristics from dual porosity model results

The inferred fracture spacing can be used to model the fluid flux in the LVC hydrothermal system. An estimate of the LVC reservoir permeability can be calculated using the depth to permeability relationship of Ingebritsen and Manning, 1999:

$$\log_{10}(k) = -14 - 3.2\log_{10}(z) \quad (8)$$

where z is the depth (km) and k is permeability (m^2). Estimates of the permeability along with the fracture spacing calculated from Sr–O isotopes can be used to quantify the mean fracture aperture using the cubic law for fracture per-

meability (Norton and Knapp, 1977; note that the dual porosity model result is not sensitive to modest changes in fracture aperture):

$$K = \frac{d^3}{12b} \tag{9}$$

where b is the fracture spacing (m), and d is the fracture aperture (m). For the LVC the reservoir depth is 0.1–0.5 km, which equates to a permeability (k) of 10^{-13} to 10^{-11} m^2. This generalized permeability compares well to the calculated minimum permeability of $10^{-13.5}$ from well 44-16 (Suemnicht, 1987). The corresponding range of fracture apertures is $10^{-4.3}$ to $10^{-3.6}$ m (0.05–0.25 mm) using a fracture spacing of 10 m.

The approximate fluid flux in the LVC hydrothermal system can also be calculated from the fracture aperture and fracture spacing. Assuming an average reservoir width of 2000 m, a thickness of 500 m and a mean fracture aperture of $10^{-3.7}$ m the cross sectional area of the fractures is 20 m^2. The fracture fluid velocities (1000–2000 m y^{-1}) yield ~600–1200 L s^{-1} for the fluid flux through the reservoir. This compares to a previous estimate of 370 L s^{-1} and current production at Casa Diablo of 850 L s^{-1} (Sorey et al., 1991; Evans et al., 2004). If the mean fracture aperture is a factor of 2 smaller (10^{-4} m) then the fluid flux would be ~300–600 L s^{-1} in the hydrothermal system.

The inferred fracture spacing of $\geqslant 10$ m has implications for the heat transfer in the system. If the average fluid velocity is 1000 m y^{-1}, then the fluid spends about 8 years traversing the 8 km distance we have evaluated with the model. The length scale for heat transfer adjacent to the fractures is, using $l \approx (Dt)^{1/2}$, about 10 m. The approximate equivalence of the inferred fracture spacing and the thermal transport distance suggests that the system is currently in steady state, and that changes in the flow rate would produce substantial changes in water temperature. The fluid cools as it traverses the system probably because the heat transferred from the fluid to the rocks is less than the heat loss from the rocks toward the Earth's surface; the latter being quite large due to the high thermal gradient (ca. 100 °C/km) between the reservoir and the surface.

6.1.4. Application of dual porosity model to Ca and Ca isotopes

The contribution of reservoir rock dissolution to the isotopic composition of Ca in the hydrothermal fluid can be calculated using the bulk reaction rate from Section 6.1.3 and Eq. (5). The change in the Ca isotope composition of the hydrothermal fluid as a function of distance is plotted in Fig. 6. The bulk reaction rate derived from the Sr-O isotope data is applied to Ca, ignoring any effects of differential mineral dissolution rates. This simplification is reasonable in the case of the LVC hydrothermal system because Ca is effectively a trace element in the Bishop Tuff (Hildreth, 1981). The model parameters and equations are identical to those used for Sr (including equal diffusivity: $D_{Ca} = D_{Sr}$) with the exception of K_{Ca}, which is set to 250 based on an average Ca concentration in the Bishop Tuff of 5000 ppm (range = 3200–6800 ppm; Hildreth, 1981) and the Ca concentration from 44-16 (19.8 ppm). The bulk reaction rate of 2.5e^{-7} g g^{-1}yr^{-1} with the flow parameters from secton 6.1.3 results in the addition of ~1.25 ng g^{-1} y^{-1}Ca due to reservoir rock dissolution. The slow rate of Ca addition and high fluid velocity means that much less than 0.1% of the total Ca in the LVC hydrothermal fluid is derived from rock dissolution. Since the calculated Ca addition due to dissolution is based on the Sr isotope-derived dissolution rate it is insensitive to the effects of secondary mineral precipitation and is the gross flux of Ca due to dissolution. The relatively small amount of Ca added during rock dissolution and the limited difference in isotopic composition means that dissolution has a minimal (<0.05‰) effect on the Ca isotopic composition of the LVC hydrothermal fluid between the West Moat (well 44-16) and the Casa Diablo well field.

East of Casa Diablo, Ca could be added to the fluid due to calcite dissolution. If calcites in the reservoir east of Casa Diablo have $^{87}Sr/^{86}Sr$ similar to the present day fluids then their dissolution would not be accounted for in the calculated dissolution rates. The dissolution of calcite with low $\delta^{44/40}Ca$ in the eastern portion of the reservoir can account for the decrease in $\delta^{44/40}Ca$ east of Casa Diablo. Mass balance calculations show that the dissolution of 7.5 μg $CaCO_3$ per gram of fluid with $\delta^{44/40}Ca = -0.5$‰ between the Casa Diablo well field and the eastern caldera wells CW-3 and 28-34 yields a hydrothermal fluid with 6 μg/g Ca and $\delta^{44/40}Ca = -0.27$‰ similar to the measured concentrations of 6.0–6.3 μg/g Ca and $\delta^{44/40}Ca = -0.23$ to -0.19‰.

6.1.5. Secondary calcite precipitation and Ca isotopes

Calcite samples from wells 57-25 and RDO-8 have low $\delta^{44/40}Ca$ compared to the co-located hydrothermal fluids (Tables 1 and 3, Fig. 7). If the sampled fluids are representative of fluids from which the calcites precipitated, this is the first observed isotopic fractionation of Ca between high temperature fluids and minerals. The change in the $\delta^{44/40}Ca$ of the hydrothermal fluid westward is complementary to the fractionation factors calculated from co-located bladed calcites and fluids assuming an isotope distillation model can be applied to the fluid samples. The similarity in the computed $\Delta^{44/40}Ca$ from calcite-fluid (-0.3‰ to -0.55‰) and a distillation model fit of the fluid data (-0.35‰) suggests that the effects of matrix rock dissolution and dispersion (including ionic diffusion) on the effective Ca isotope fractionation factor in the fluid are minimal.

Sustained calcite saturation and subsequent precipitation in hydrothermal fluids is commonly attributed to increasing alkalinity from reservoir mineral dissolution or CO_2 degassing during phase separation (Simmons and Christenson, 1994). The solubility of calcite is sensitive to the changes in carbonate speciation during the degassing or boiling of hydrothermal fluids (Simmons and Christenson, 1994). The observed rapid decline in Ca and CO_2 concentrations and concomitant increase in $\delta^{44/40}Ca$ (Fig. 3) is consistent with calcite precipitation being due to degassing. Moreover, the bladed textures of the LV hydrothermal calcites are consistent with vapor loss-induced precipitation and relatively rapid (and hence non-equilibrium) mineral growth (Simmons and Christenson, 1994; Wollenberg, 1987). Thermodynamic models and mass balance calcula-

tions suggest that calcite precipitates during CO_2 degassing and minor feldspar dissolution (Tempel et al., 2011). The conclusions of Tempel et al. (2011) are consistent with our larger, more complete dataset.

We conclude that the LVC fluids and calcites document high temperature Ca stable isotope fractionation similar in magnitude, or slightly smaller than, that observed for low temperature inorganic calcite (e.g., Tipper et al., 2006; Tang et al., 2008a,b). Our observation indicates that precipitation of hydrothermal minerals can take place under non-equilibrium conditions, possibly as a result of the effects of degassing of CO_2 as noted above. Such kinetic fractionation could also apply to O isotopes, although a 0.5‰ effect is unlikely to change the interpretation of those data significantly.

6.2. Equilibrium versus kinetic fractionation during calcite precipitation

Although we argue that the observed fractionation of Ca isotopes in hydrothermal calcites from Long Valley is a kinetic effect, it is also true that the equilibrium Ca isotope fractionation factor is not known except at low temperature and only by inference from comparison of coexisting calcite and pore fluids in deep sea carbonates and groundwaters. However, because the inferred fractionation factor at low temperature (5–25 °C) is unity ($\alpha = 1.0000$; Fantle and DePaolo, 2007; Jacobson and Holmden, 2008) it is likely that the equilibrium fractionation factor at higher temperature is also unity. This follows from the fact that the equilibrium fractionation factor generally has an asymptotic relationship with temperature:

$$\ln(\alpha_{eq}) \propto \frac{1}{T^2} \tag{10}$$

so the absolute value of $\ln(\alpha_{eq})$ decreases with increasing temperature.

At low temperatures, the partitioning of Sr relative to Ca also is kinetically controlled and varies as a function of precipitation rate (Lorens, 1981; Tesoriero and Pankow, 1996; Tang et al., 2008a,b). The dependence on precipitation rate is such that the equilibrium Sr/Ca distribution coefficient can be approached in laboratory experiments, and the value at equilibrium is likely to be about 0.03 ± 0.01 (cf. DePaolo, 2011; Nielsen et al., 2013).

One LVC calcite sample (massive calcite from 1844 ft in RDO-8 drill core) has $\Delta^{44/40}$Ca of zero and hence may have precipitated close to equilibrium. The remaining 3 samples plot distinctly outside the likely equilibrium range (Fig. 7). The near equilibrium $\Delta^{44/40}$Ca and K_{Sr} for RDO-8-1844 cc is consistent with the textural observations of Simmons and Christenson (1994) for hydrothermal calcite grown during dissolution-precipitation reactions whereas the remaining samples are chemically and texturally consistent with kinetically controlled growth.

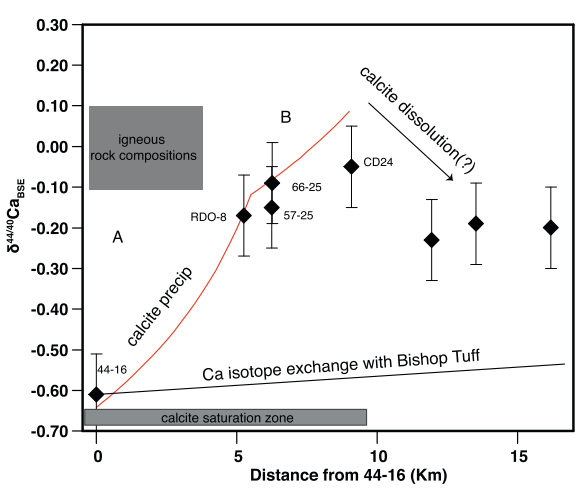

Fig. 6. Proposed model for Ca isotope evolution in the LVC hydrothermal fluid. The model curve assumes that the effect of dissolution and mixing on the Ca concentration and isotope ratio is negligible and that the isotope composition can be modeled as a Rayleigh distillation process ($\alpha = 0.9957$). Segment A has a Ca precipitation rate of 12.8% km^{-1}, segment B has a Ca precipitation rate of 3.2% km^{-1}. East of well CD24 older secondary calcites are likely dissolving, lowering the $^{44/40}$Ca of the fluids. Additionally the reduction in calcite supersaturation may reduce the fractionation factor between the Basalt Canyion wells (57-25 and 66-25) and the main Casa Diablo well field (CD24; e.g., Tang et al., 2008a).

6.2.1. Kinetically limited calcite growth

The negative values of $\Delta^{44/40}$Ca and the non-equilibrium K_{Sr} for LVC hydrothermal calcites requires kinetic control on calcite precipitation. Kinetic effects could include both transport-limited fractionation in the fluid phase (diffusion) and surface reaction effects (e.g., Watson, 2004; Watson and Müller, 2009; DePaolo, 2011). Diffusive fractionation of Ca isotopes during growth of LVC calcites is unlikely because the solutions have [Ca] >> [CO_3] (10–100) (cf. DePaolo, 2011).

Isotope and trace element fractionation during ion dehydration is thought to be the rate-limiting step in crystal surface-limited growth, and in such a case the light isotope will be preferentially dehydrated at the mineral growth surface (e.g., Lippman, 1960; Fantle and DePaolo, 2007; DePaolo, 2011; Hofmann et al., 2012). Similarly, trace element incorporation during rate-dependent growth might be dependent on the dehydration rates of trace metals compared to stoichiometric mineral components. The precise mechanism that favors the preferential dehydration of light isotopes is not known, but an area of active research (e.g., Hofmann et al., 2012).

Fig. 7 shows the $\Delta^{44/40}$Ca and K_{Sr} data for the LVC calcites fitted using the model of DePaolo (2011). The fitting parameters are $\alpha_{eq} = 1.0000$, $\alpha_f = 0.99945$, $K_{eq(Sr)} = 0.03$ and $K_{f(Sr)} = 0.8$. The low temperature calcite precipitation experiments of Tang et al. (2008a,b) are shown for comparison. To apply the DePaolo (2011) model we need an estimate for the background exchange rate (R_b), which is estimate from the calcite dissolution rate of is $10^{-4.25}$ mol m^{-2} s^{-1} at 150 °C (Pokrovsky et al., 2009). At $pCO_2 < 10$ bars and pH ~ 5 calcite dissolution rates are reasonably invariant between 60 and 150 °C. The true back-

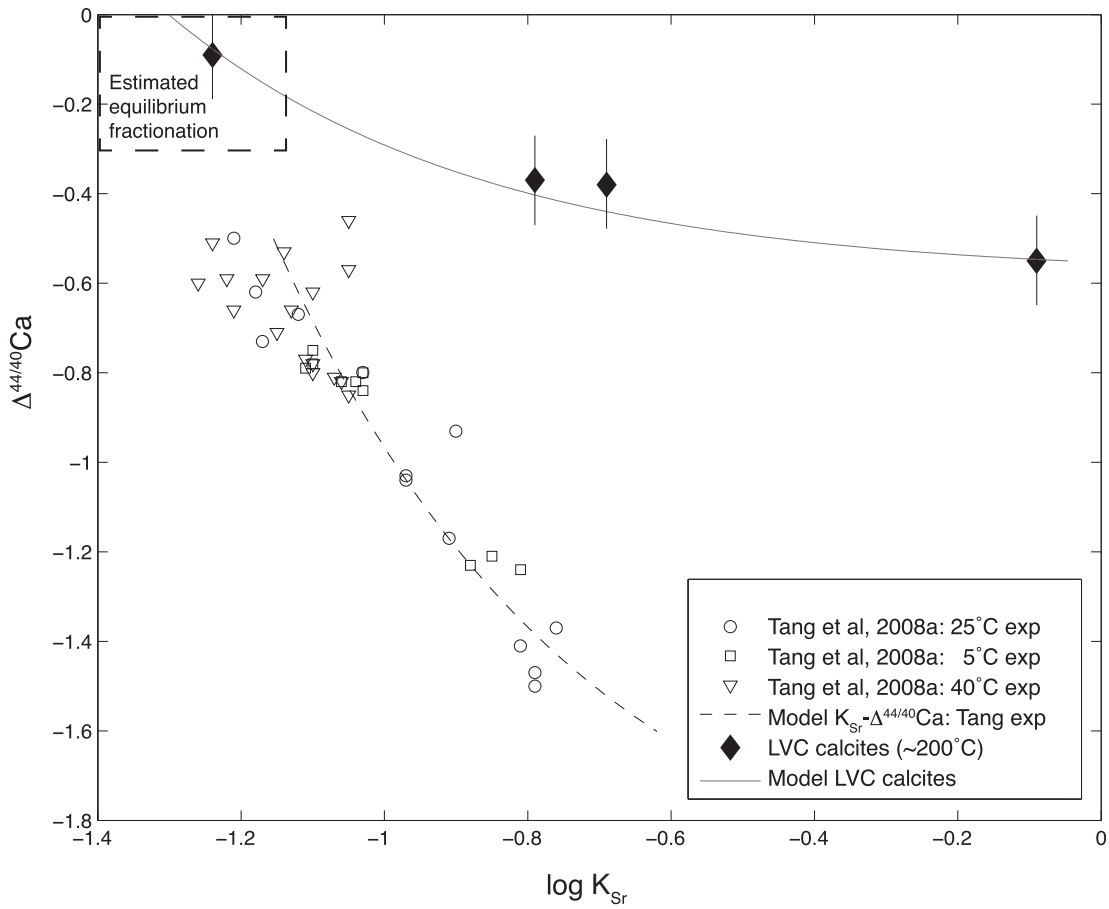

Fig. 7. Covariations in Δ^{44}Ca and D_{Sr} for calcites from LVC hydrothermal fluids. The sample from 57-25, samples RDO-8-1191 and RDO-8-1204 are bladed calcites, texturally consistent with precipitation during phase separation while RDO-8-1844 is a massive calcite, texturally consistent with precipitation in a low fluid: rock environment. Low temperature experimental studies suggest variations in in Δ^{44}Ca and D_{Sr} are due to changes in the precipitation rate of calcite. Both curves are fit to the data using the DePaolo (2011) model with the fitting parameters described in the text.

ground exchange rate is a complex function of calcite saturation, solution chemistry, ionic strength, pH and pCO_2 as is the case for calcite dissolution, however DePaolo (2011) demonstrated that experimentally determined dissolution rates are reasonable approximations for the purpose of modeling isotope and trace element fractionation.

The primary observation from Fig. 7 is the correlation between K_{Sr} and $\Delta^{44/40}$Ca for the LVC calcites, which is analogous to effects observed in low temperature, growth rate dependent experiments (Tang et al., 2008a; Tang et al., 2008b). In detail, K_{Sr} variations for LVC calcites are greater and $\Delta^{44/40}$Ca range is more restricted than at low temperature (Fig. 7). The change in slope may be due to some fundamental change in the chemistry of Sr or Ca in solution or other solution chemistry parameters that have not been yet linked to trace element or Ca isotope fractionation experimentally. For example changes in coordination number or the hydration number may affect the relative fractionation of Ca isotopes and Sr/Ca. The kinetic limit α_f from Fig. 6 is equal to the diffusion controlled fractionation factor for Ca isotopes (Bourg et al., 2010). While the Ca/CO_3 of the hydrothermal fluid suggests that diffusion should not control Ca isotope fractionation however a role for diffusive isotope fractionation cannot be completely ruled out.

7. CONCLUSIONS

Isotopic variability of fluids from the shallow hydrothermal system in Long Valley Caldera is the result of fluid–fluid mixing, and precipitation-dissolution reactions. The bulk rock dissolution rate is determined from the variations in Sr and O isotopes along the fluid flow path. Isotopes of Ca are fractionated during calcite precipitation at hydrothermal temperatures. The maximum observed fractionation of $^{44}Ca/^{40}Ca$ is 0.55‰, which is approximately ¼ of the maximum observed kinetic fractionation observed in low temperature experiments and natural samples. It is unclear whether this represents a maximum fractionation factor at hydrothermal conditions; however, it supports the idea that primary controls on kinetic fractionation factors are the forward and backward precipitation rates and not temperature.

ACKNOWLEDGEMENTS

Support for S.T.B., B.M.K and D.J.D was provided by the Director, Office of Science, Office of Basic Energy Sciences, of the U.S. Department of Energy and the Assistant Secretary for Energy Efficiency and Renewable Energy, Office of Geothermal Technologies, of the U.S. Department of Energy under Contract No. DE-AC02-05CH11231. The U.S. Geological Survey Volcano Hazards and Geothermal Resources programs supported Shaul Hurwitz and Bill Evans. John Ferry and Larry Nickerson generously provided samples. Joe Moore provided access to the RDO-8 drill core through the EGI core repository at the University of Utah. Analytical support at Berkeley/LBNL from Markus Bill, Wenbo Yang and Tom Owens is gratefully acknowledged. Thorough reviews by Ed Tipper and two anonymous reviewers improved the manuscript. An informal review and discussions with Jim Watkins sharpened our thinking about mineral growth and associated geochemical characteristics of fluids and minerals.

APPENDIX A. SUPPLEMENTARY DATA

Supplementary data associated with this article can be found, in the online version, at http://dx.doi.org/10.1016/j.gca.2013.08.011.

REFERENCES

Alt J. C. (1995) Subseafloor processes in mid-ocean ridge hydrothermal systems. In *Seafloor Hydrothermal Systems: Physical, Chemical, and Biological Interactions, Geophys. Monogr.*, vol. 91 (eds. S. Humphris, J. Lupton, L. Mullineaux and R. Zierenberg). AGU, Washington, DC, pp. 85–114.

Bailey R. A., Dalrymple G. B. and Lanphere M. A. (1976) Volcanism, structure and geochronology of the Long Valley caldera, Mono County, California. *J. Geophys. Res.* **81**(5), 725–744.

Baxter E. and DePaolo D. J. (2000) Field evidence for slow metamorphic reaction rates at 500–600 °C. *Science* **288**, 1411–1414.

Bergfeld D., Evans W. C., Howle J. F. and Farrar C. D. (2006) Carbon dioxide emissions from vegitation-kill zones around the resurgent dome of Long Valley caldera, eastern California, USA. *J. Volcanol. Geotherm. Res.* **152**, 140–156.

Bourg I. C., Richter F. M., Christensen J. N. and Sposito G. (2010) Isotopic mass-dependence of metal cation diffusion coefficients in liquid water. *Geochim. Cosmochim. Acta* **74**, 2249–2256.

Brown S. T., DePaolo D. J., Turchyn A. V., Kennedy B. M., Alt J. C., Bedard J. and Skulski T. (2009) Calcium Isotope Fractionation in Hydrothermal Systems. *American Geophysical Union Fall Meeting Abstracts*.

Brown S. T., DePaolo D. J., Turchyn A. V. and Alt J. C. (2010) Calcium Isotope Fractionation in ocean ridge hydrothermal systems. *Geochim. Cosmochim. Acta* **A125**.

Caro G., Papanastassiou D. A. and Wasserburg G. J. (2010) 40K–40Ca isotopic constraints on the oceanic calcium cycle. *Earth Planet. Sc. Lett.* **296**(1–2), 124–132.

Christensen J. N. and DePaolo D. J. (1993) Time scales of large volume silicic magma systems: Sr isotopic systematics of phenocrysts and glass from the Bishop Tuff, Long Valley, California. *Contrib. Mineral. Petrol.* **113**, 100–114.

Coumou D., Driesner T. and Heinrich C. A. (2008) The structure and dynamics of mid-ocean ridge hydrothermal systems. *Science* **321**, 1825–1828.

Craig H. (1961) Isotopic variations in meteoric waters. *Science* **133**, 1702–1703.

Craig H., Boato G. and White D. E. (1956) Isotopic geochemistry of thermal waters. *Proc. Second Natl. Acad. Sci.* **19**, 29–44.

DePaolo D. J. (2004) Calcium isotopic variations produced by biological, kinetic, radiogenic and nucleosynthetic processes. *Rev. Mineral. Geochem.* **55**(1), 255–288.

DePaolo D. J. (2006) Isotope effects in fracture-dominated reactive fluid-rock systems. *Geochim. Cosmochim. Acta* **70**, 1077–1096.

DePaolo D. J. (2011) Surface kinetic model for isotopic and trace element fractionation during precipitation of calcite from aqueous solutions. *Geochim. Cosmochim. Acta* **75**, 1039–1056.

Doe B. R. and Zartman R. E. (1979) Plumbotectonics I, The Phanerozoic. In *Geochemistry of Hydrothermal Ore Deposits* (ed. H. L. Barnes), second ed. Wiley Interscience, pp. 22–70.

Eastoe C. J. and Guilbert J. M. (1992) Stable chlorine isotopes in hydrothermal processes. *Geochim. Cosmochim. Acta* **56**(12), 4247–4255.

Elderfield H. and Schultz A. (1996) Mid-ocean ridge hydrothermal fluxes and the chemical composition of the ocean. *Ann. Rev. Earth Planet. Sci.* **24**, 191–224.

Evans W. C., Banks N. G. and White L. D. (1981) Analyses of gas samples from the summit crater. In *The 1980 Eruptions of Mount St. Helens*, vol. 1250 (eds. P. W. Lipman and D. R. Mullineaux). U.S. Geological Surv. Prof. Pap., Washington, pp. 227–232.

Evans W. C., White L. D. and Rapp J. B. (1988) Geochemistry of some gases in hydrothermal fluids from the southern Juan de Fuca Ridge. *J. Geophys. Res.* **93**, 15305–15313.

Evans W. C., Sorey M. L., Cook A. C., Kennedy B. M., Shuster D. L., Colvard E. M., White L. D. and Huebner M. A. (2002). *J. Volcanol. Geotherm. Res.* **114**, 1–22.

Evans W. C., Lorenson T. D., Sorey M. L. and Bergfeld D. (2004) Transport of injected isobutane by thermal groundwater in Long Valley caldera, California, USA. In *Water-Rock Interaction-11* (eds. R. B. Wanty and R. R. Seal II), pp. 125–129.

Fantle M. S. and DePaolo D. J. (2006) Sr isotopes and pore fluid chemistry in carbonate sediment of the Ontong Java Plateau: Calcite recrystallization rates and evidence for a rapid rise in seawater Mg over the last 10 million years. *Geochim. Cosmochim. Acta* **70**(15), 3883–3904.

Fantle M. S. and DePaolo D. J. (2007) Ca isotopes in carbonate sediment and pore fluid from ODP Site 807A: the Ca2+(aq)-calcite equilibrium fractionation factor and calcite recrystallization rates in Pleistocene sediments. *Geochim. Cosmochim. Acta* **71**, 2524–2546.

Farkus J., Bohm F., Wallmann K., Blenkinsop J., Eisenhauer A., van Geldern R., Munnecke A., Voigt S. and Veizer J. (2007) Calcium isotope record of Phaerozoic oceans: Implications for chemical evolution of seawater and its causative mechanisms. *Geochim. Cosmochim. Acta* **71**, 5117–5134.

Farmer G. L. and DePaolo D. J. (1987) Nd and Sr isotope study of hydrothermally altered granite at San Manuel, Arizona: implications for element migration paths during the formation of porphyry copper ore deposits. *Econ. Geol.* **82**.

Farmer G. L. and DePaolo D. J. (1997) Sources of Hydrothermal Components: Heavy Isotopes. In *The Geochemistry of Hydrothermal Ore Deposits* (ed. H. L. Barnes). Wiley Interscience, pp. 31–61.

Ferry J. M., Boswell A. W. and Rumble D. (2001) Formation of wollastonite by chemically reactive fluid flow during contact metamorphism, Mt. Morrison Pendant, Sierra Nevada, California, USA. *J. Petrol.* **42**(9), 1075–1728.

Flexser S. (1991) Hydrothermal alteration and past and present thermal regimes in the western moat of Long Valley caldera. *J. Volcanol. Geotherm. Res.* **48**, 303–318.

Goff F., Wollenberg H. A., Brookins D. C. and Kistler R. W. (1991) A Sr-Isotopic comparison between thermal waters, rocks and hydrothermal calcites, Long Valley caldera, California. *J. Volcanol. Geotherm. Res.* **48**, 265–281.

Halliday A. N., Fallick A. E., Hutchinson J. and Hildreth W. (1984) A Nd, Sr and O isotopic investigation into the causes of chemical and isotopic zonation in the Bishop Tuff, California. *Earth Planet. Sci. Lett.* **68**, 379–391.

Hildreth W. (1979) The Bishop Tuff: evidence for the origin of compositional zonation in silicic magma chambers. In *Ash-Flow Tuffs*, vol. 180 (eds. C. E. Chapin and W. E. Elston). Geological Society of America Special Paper, pp. 43–72.

Hildreth E. W. (1981) Gradients in silicic magma chambers: implications for lithospheric magmatism. *J. Geophys. Res.* **86**, 10153–10192.

Hildreth W. (2004) Volcanological perspectives on Long Valley, Mammoth Mountain and Mono Craters: several contiguous but discrete systems. *J. Volcanol. Geotherm. Res.* **136**, 169–198.

Hilton D. R. (1996) The helium and carbon isotope systematics of a continental geothermal system: Results from monitoring studies at Long Valley caldera (California, USA). *Chem. Geol.* **127**, 269–295.

Hofmann A. E., Bourg I. C. and DePaolo D. J. (2012) Ion desolvation as a mechanism for kinetic isotope fractionation in aqueous systems. *PNAS* **109**, 18,689–18,694.

Hurwitz S., Farrar C. D. and Williams C. F. (2010) The Thermal regime in the Resurgent Dome of Long Valley Caldera, California, Inferences from precision temperature logs in deep wells. *J. Volcanol. Geotherm. Res.* **198**, 233–240.

Ingebritsen S. E. and Manning C. E. (1999) Geological implications of a permeability-depth curve for the continental crust. *Geology* **27**, 1107–1110.

Jacobson A. D. and Holmden C. (2008) $D^{44}Ca$ evolution in a carbonate aquifer and its bearing on the equilibrium isotope fractionation factor for calcite. *Earth Planet. Sci. Lett.* **270**, 349–353.

Jacobson A. D. and Wasserburg G. J. (2005) Anhydrite and the Sr isotope evolution of groundwater in a carbonate aquifer. *Chem. Geol.* **214**, 331–350.

Johnson T. M. and DePaolo D. J. (1994) Interpretation of isotopic data in groundwater-rock systems: model development and application to Sr isotopic data from Yucca Mountain. *Water Resour. Res.* **30**, 1571–1587.

Kaufmann R., Long A., Bentley H. and Davis S. (1984) Natural chlorine isotope variations. *Nature* **309**, 338–340.

Kharaka Y. K., Gunter W. D., Aggarwal P. K., Perkins E. H. and DeBraai J. D. (1988) SolMINEQ88: a computer program for geochemical modeling of water-rock interactions. *US. Geol. Surv., Water Resour. Invest.* **88-4227**, 420.

Kistler R. W. and Peterman Z. E. (1973) Variations in Sr, Rb, K and Na and initial $^{87}Sr/^{86}Sr$ in Mesozoic granitic rocks and intruded wall rocks in central California I. Geology and petrology: summary. *Geol. Soc. Am. Bull.* **91**, 515–518.

Kistler R. W., Chappell B. W., Peck D. L. and Bateman P. C. (1986) Isotopic variation in the Tuolumne Intrusive Suite, central Sierra Nevada, California. *Contrib. Mineral. Petrol.* **94**, 205–230.

Lackey J. S. and Valley J. W. (2004) Complex patterns of fluid flow during wollastonite formation in calcareous sandstones at Laurel Mountain, Mt. Morrison Pendant, California. *GSA Bull.* **116**, 76–93.

Langmuir C., Vocke R., Hanson G. and Hart S. (1978) A general mixing equation with applications to Icelandic basalts. *Earth Planet. Sci. Lett* **37**, 380–392.

Lemarchand D., Wasserburg G. J. and Papanastassiou D. A. (2004) Rate-controlled calcium isotope fractionation in synthestic calcite. *Geochim. Cosmochim. Acta* **68**(22), 4665–4678.

Lippman F. (1960) *Sedimentary Carbonate Minerals*. Springer-Verlag, New York, 228 p.

Lorens R. (1981) Sr, Cd, Mn and Co distribution coefficients in calcite as a function of calcite precipitation rate. *Geochim. Cosmochim. Acta* **45**, 553–561.

Mahood G. A., Ring J. H., Manganelli S. and McWilliams M. O. (2010) New $^{40}Ar/^{39}Ar$ ages reveal contemporaneous mafic and silicic eruptions during the past 160,000 years at Mammoth Mountain and Long Valley caldera, California. *GSA Bull.* **122**, 3.

Magaritz M. and Taylor H. P. (1976) Isotopic evidence for meteoric hydrothermal alteration of plutonic igneous rocks in Yakutat Bay and Skagway areas, Alaska. *Earth Planet. Sci. Lett.* **30**, 179–190.

Maloszewski P. and Zuber A. (1991) Influence of matrix diffusion and exchange reactions on radiocarbon ages in fissured carbonate aquifers. *Water Resour. Res.* **27**, 1937–1945.

Masi U., O'neil J. R. and Kistler R. W. (1981) Stable isotope systematics in mesozoic granites of Central and Northern California and Southwestern Oregon. *Contrib. Mineral. Petrol.* **76**, 116–126.

McConnell V. S., Valley J. W. and Eichelberger J. C. (1997) Oxygen Isotope composition of intracaldera rocks: hydrothermal history of the Long Valley Caldera, California. *J. Volcanol. Geotherm. Res.* **76**, 83–109.

Nielsen L. C., Druhan J. L., Brown S. T., Yang W. and DePaolo D. J. (2011) Chapter 9: Calcium isotopes as tracers of biogeochemical processes. In *Handbook of Environmental Isotope Geochemistry* (ed. M. Baskaran), first ed. Springer.

Nielsen L. C., DePaolo D. J. and DeYoreo J. J. (2012) Self-consistent ion-by-ion growth model for kinetic isotopic fractionation during calcite precipitation. *Geochim. Cosmochim. Acta* **86**, 166–181.

Nielsen L. C., De Yoreo J. J. and DePaolo D. J. (2013) General model for calcite growth kinetics in the presence of impurity ions. *Geochim. Cosmochim. Acta* **115**, 100–114.

Norton D. and Knapp R. (1977) Transport phenomena in hydrothermal systems: the nature of porosity. *Am. J. Sci.* **227**, 913–936.

Ohmoto (1972) Systematics of sulfur and carbon isotopes in hydorthermal ore deposits. *Econ. Geol.* **67**(5), 551–578.

Pokrovsky O. S., Golubev S. V., Schott J. and Castillo A. (2009) Calcite, dolomite and magnesite dissolution kinetics in aqueous solutions at acid to circum neutral pH, 25 to 150 °C and 1 to 55 atm pCO2: new constraints on CO2 sequestration in sedimentary basins. *Chem. Geol.* **265**, 20–32.

Révész, Kinga and Coplen T.B. (2008a) Determination of the delta (2H/1H) of water: RSIL lab code 1574. In *Methods of the Reston Stable Isotope Laboratory* (eds. Révész, Kinga, and Coplen, T.B.), Chap. C1. U.S. Geological Survey Techniques and Methods 10–C1, 27 p. Available from: <http://pubs.water.usgs.gov/tm10C1/>.

Révész, Kinga and Coplen, Tyler B. (2008b) Determination of the delta ($^{18}O/^{16}O$) of water: RSIL lab code 489. In *Methods of the Reston Stable Isotope Laboratory* (eds. Révész, Kinga, and Tyler B. Coplen), chap. C2. U.S. Geological Survey Techniques and Methods, 10–C2, 28 p. Available from: <http://pubs.water.usgs.gov/tm10C2/>.

Richter F. M. and DePaolo D. J. (1988) Diagenesis and Sr isotopic evolution of seawater using data from DSDP 590B and 575. *Earth Planet Sci. Lett.* **90**, 382–394.

Ryu J.-S., Jacobson A. D., Holmden C., Lundstrom C. and Zhang Z. (2011) The major ion, $d^{44/40}Ca$, $d^{44/42}Ca$, and d26/24Mg

geochemistry of granite weathering at pH = 1 and $T = 25\,°C$: power-law processes and the relative reactivity of minerals. *Geochim. Cosmochim. Acta* **75**, 6004–6026.

Sanford W. (1997) Correcting for diffusion in carbon-14 dating of groundwater. *Ground Water* **35**, 357–361.

Sarna-Wojcicki A. M., Pringle M. S. and Wijbrans J. (2000) New 40Ar/39Ar age of the Bishop Tuff from multiple sites and sediment rate calibration for the Matuyama–Brunhes boundary. *J. Geophys. Res.* **105**(B9), 21431–21444.

Simmons S. F. and Christenson B. F. (1994) Origins of calcite in a boiling geothermal system. *Am. J. Sci.* **294**, 361–400.

Simon J. I. and DePaolo D. J. (2010) Stable calcium isotopic composition of meteorites and rocky planets. *Earth Planet. Sci. Lett.* **289**, 457–466.

Skelton A. D. L., Bickle M. J. and Graham C. M. (1997) Fluid-flux and reaction rate from advective-diffusive carbonation of mafic sill margins in the Dalradian, southwest Scottish Highlands. *Earth Planet. Sci. Lett.* **146**, 527–539.

Skulan J., DePaolo D. J. and Owens T. L. (1997) Biological control of calcium isotopic abundances in the global calcium cycle. *Geochim. Cosmochim. Acta* **61**, 2505–2510.

Sorey M. L., Suemnicht G. A., Sturchio N. J. and Nordquist G. A. (1991) New evidence on the hydrothermal system in Long Valley caldera, California, from wells fluid sampling, electrical geophysics and age determinations of hot spring deposits. *J. Volcanol. Geotherm. Res.* **48**, 229–263.

Suemnicht G. A. (1987) Results of deep drilling in the western moat of long valley, California. *EOS* **68**(785), 798.

Suemnicht G. A., Sorey M. L., Moore J. N., and Sullivan R. (2007) The Shallow Hydrothermal system of Long Valley Caldera, California. *Thirty-Second Workshop on Geothermal Reservoir Engineering*.

Tang J., Deitzel M., Bohm F., Kohler S. J. and Eisenhauer A. (2008a) Sr^{2+}/Ca^{2+} and $^{44}Ca/^{40}Ca$ fractionation during inorganic calcite formation: II. Ca isotopes. *Geochim. Cosmochim. Acta* **72**, 3733–3745.

Tang J., Kohler S. J. and Deitzel M. (2008b) Sr2+/Ca2+ and $^{44}Ca/^{40}Ca$ fractionation during inorganic calcite formation: I. Sr incorporation. *Geochim. Cosmochim. Acta* **72**, 3718–3732.

Taylor H. P. (1974) The application of oxygen and hydrogen isotope studies to problems of hydrothermal alteration and ore deposition. *Econ. Geol.* **69**, 757–776.

Taylor H. P. (1977) Water/rock interaction and the origin of H2O in granitic batholiths. *J. Geol. Soc. London* **133**, 509–588.

Taylor H. P. and Forester R. W. (1979) An oxygen and hydrogen isotope study of the Skaergaard intrusion and its country rocks: a description of a 55 M.Y. old fossil hydrothermal system. *J. Petrol.* **20**(3), 355–419.

Tempel R. N., Sturmer D. M. and Schiling J. (2011) Geochemical modeling of the near surface hydrothermal system beneath the southern moat of Long Valley Caldera, California. *Geothermics* **40**, 91–101.

Tesoriero A. and Pankow J. (1996) Solid solution partitioning of Sr^{2+}, Ba^{2+}, and Cd^{2+} to calcite. *Geochim. Cosmochim. Acta* **60**, 1053–1063.

Tipper E. T., Galey A. and Bickle M. J. (2006) Riverine evidence for a fractionated reservoir of Ca and Mg on the Continents: implications for the oceanic Ca cycle. *Earth Planet. Sci. Lett.* **247**, 267–279.

Watson E. B. (2004) A conceptual model for near-surface kinetic controls on the trace-element and stable isotope composition of abiogenic calcite crystals. *Geochim. Cosmochim. Acta* **68**, 1473–1488.

Watson E. B. and Müller T. (2009) Non-equilibrium isotopic and elemental fractionation during diffusion-controlled crystal growth under static and dynamic conditions. *Chem. Geol.* **267**, 111–124.

White A. F. and Peterson M. L. (1991) Chemical equilibrium and mass balance relationships assoicated with the Long Valley hydrothermal system, California, USA. *J. Volcanol. Geotherm. Res.* **48**, 283–302.

White A. F., Peterson M. L., Wollenberg H. A. and Flexser S. (1990) Sources and fractionation processes influencing the isotopic distribution of H, O, and C in the Long Valley hydrothermal system, California, USA. *Appl. Geochem.* **5**, 571–585.

Wollenberg H. (1987) *A Core Hole into the Hydrothermal System of the Long Valley Caldera*. LBNL report # 24569.

Associate editor: Edward M. Ripley